

## Emittance growth due to space charge compensation and beam intensity instabilities in negative ion beams

C. A. Valerio-Lizarraga\*

Facultad de Ciencias Físico-Matemáticas Universidad Autónoma de Sinaloa,  
CP. 80010, Culiacán, México



(Received 22 September 2017; published 8 March 2018)

The need to extract the maximum beam intensity with low transversal emittance often comes with the drawback of operating the ion source to limits where beam current instabilities arise, such fluctuations can change the beam properties producing a mismatch in the following sections of the machine. The space charge compensation (SCC) generated by the beam particles colliding with the residual gas reaches a steady state after a build-up time. This paper shows how once in the steady state, the beam ends with a transversal emittance value bigger than the case without compensation. In addition, we study how the beam intensity variation can disturb the SCC dynamics and its impact on the beam properties. The results presented in this work come from 3-D simulations using tracking codes taking into account the secondary ions to estimate the degree of the emittance growth due to space charge and SCC.

DOI: 10.1103/PhysRevAccelBeams.21.030101

### I. INTRODUCTION

Several mechanisms impede the ion source to deliver a beam with constant properties along the pulse, mainly when the accelerator applications demand intensities beyond the ion source capacity to provide steady beams [1]. This situation can affect the machine operation, where the beam intensity can vary along the pulse [2] producing changes in other parameters like the transversal emittance.

The space charge compensation (SCC) occurs when the beam ionizes the residual gas inside the vacuum chamber producing electrons and positive ions. Negative beams collect the positive ions by the electric potential, then the local charge density decreases and therefore the electric field inside the beam also decreases. The electrons produced in the ionization are expelled to the walls and do not contribute to the SCC. In this work, we refer secondary particles to the positive ions.

The current instability by itself limits the beam transport and also affects the SCC dynamics, because the total charge to be compensated changes and the SCC process takes some time to stabilize and instead of improving the beam dynamics, it can have an adverse effect by enhancing the beam instabilities effect in the transport.

To quantify the current instabilities and SCC effects, we will concentrate our study on negative beams ( $H^-$ ,  $Li^-$ , and  $D^-$ ) traveling inside a drift section and later add a solenoid magnet to compare its impact. The simulations used for this work previously have demonstrated a proper matching with measurements even in the presence of magnetic fields [3].

### II. SPACE CHARGE COMPENSATION PARAMETERS

The mean free path [Eq. (1)] for the process of a beam particle colliding with the residual gas is determined by the gas density ( $n_g$ ) and the cross section of residual gas ionization [ $\sigma(E)$ ] by primary ions which is a function of the ion kinetic energy  $E$  [4].

$$L = \frac{1}{n_g \cdot \sigma(E)} \quad (1)$$

By dividing Eq. (1) by the beam velocity ( $v_b$ ), we obtained the required time to create one secondary ion for every beam particle [Eq. (2)]. The SCC characteristic time  $\tau$  corresponds to the minimum time needed for the SCC process to collect the necessary ions and reach a steady state, but secondary ion losses can increase the required time to compensate the beam.

$$\tau = \frac{1}{n_g \cdot \sigma(E) \cdot v_b}. \quad (2)$$

In the period  $t < \tau$ , the SCC leads to variations in the beam properties [5] that complicates the beam matching until the beam is compensated and reaches the steady state.

\*cvalerio@uas.edu.mx

Published by the American Physical Society under the terms of the *Creative Commons Attribution 4.0 International* license. Further distribution of this work must maintain attribution to the author(s) and the published article's title, journal citation, and DOI.

Multiple experiments report how the beam is not fully neutralized even after reaching the steady state [6,7], leaving a residual electric potential. We only studied the beam dynamics after  $\tau$ .

Because our study is limited to gas densities where the electric potential keeps its negative sign, and the simulation time is less than one millisecond, we neglect the recombination of electrons with secondary ions [5].

To quantify the SCC degree, we introduced the function  $\eta$ , where the Eq. (3) presents its definition, this depends on the ratio of the potential in the center of the compensated beam ( $\phi_B$ ) and the potential created by an uncompensated beam following the same trajectory ( $\phi_{NC}$ ).

$$\eta = 1 - \frac{\phi_B(z, t)}{\phi_{NC}(z, t)} \quad (3)$$

The compensation degree in the steady state depends on the secondary particles loss mechanism and the beam potential well determined by the system constraints. Overcompensation appears when the gas density is so high that the secondary ions creation rate overcomes the beam density creating a positive potential.

Only the  $H_2$  residual gas is considered to carry the SCC because it is the most common residual gas in vacuum systems. Other gases like Kr can be used to help the compensation, but in general they need to be injected into the system [3], meanwhile  $H_2$  can appear naturally.

A  $50 \mu s$   $\tau$  was selected to study the beam instabilities under SCC for the  $H^-$  beam. Using Eq. (2) the equivalent  $H_2$  residual gas pressures is  $2 \times 10^{-5}$  mbar inside the vacuum system. At this pressure there is not an overcompensation in the beam potential [3] and the stripping losses are below 4% [8].

Equation (4) describe the beam potential radial solution for a DC beam, where  $R$  is the beam radius,  $b$  the beam vacuum pipe radius,  $I_b$  the beam current and  $v_b$  the beam velocity. For a fixed  $R$  and  $b$ , this shows how the electric potential will increase linearly with the current.

$$\phi(r) = \begin{cases} \frac{2I_b}{v_b} \left( \frac{r^2}{2R^2} + \ln\left(\frac{R}{b}\right) - \frac{1}{2} \right) & 0 \leq r \leq R \\ \frac{2I_b}{v_b} \left( \ln\left(\frac{r}{b}\right) \right) & R \leq r \leq b. \end{cases} \quad (4)$$

We propose to study the SCC where the beam energy for all the beam ions will be the same ( $E = C$ ). By using the classic beam kinetic energy definition  $E = \frac{1}{2} m v_b^2$  then taking the beam energy as constant  $v_b = C \sqrt{1/m_b}$ , we can use Eq. (2) to obtain

$$\tau = \frac{\sqrt{m_b}}{[n_{H_2} \cdot \sigma_{H_2}(E) \cdot C]} \quad (5)$$

Assuming the same cross section for all the beam ions, the following can be interpreted as heavier the beam particle, the longer it takes to compensate the beam.

Also Eq. (4) states how the beam potential will increase as the beam velocity decreases.

### III. SIMULATIONS

The Ion Beam Simulator (IBSIMU) [9] code has been extensively used in several experiments with fair matching between simulations and measurements of extraction systems [10,11], and recently in beam transport and SCC calculations [3].

The code IBSIMU calculates the electric field and takes into account the beam space charge in the following way: First, it creates a 3-D mesh to allocate the geometry that calculates the electric potential distribution by solving the Laplace equation  $\nabla^2 \phi = 0$  for the boundary conditions (Neumann and Dirichlet), using finite difference method (Fig. 1).

In the next step, a multiparticle beam is tracked (the initial beam conditions are defined) through the potential generated in the previous step, as well as any present magnetic field. The tracked beam particles generate a space charge density map.

The space charge map is used to calculate the potential distribution on the nodes of the mesh [12] by solving the nonlinear Poisson-Vlasov system with the beam density for the Poisson equation as  $\nabla^2 \phi = -\rho_b / \epsilon_0$ .

The beam is tracked again from its initial conditions in the electric potential derived from the Poisson solution. This process repeated itself until the result converges to a self-consistent solution as shown in Fig. 1.

The previous electric potentials represent the solution for a beam traveling in a perfect vacuum. If we want to model the SCC effect we can take two approaches: (1) Net current model: In this simple model we decrease the beam current to simulate the impact of the SCC without including

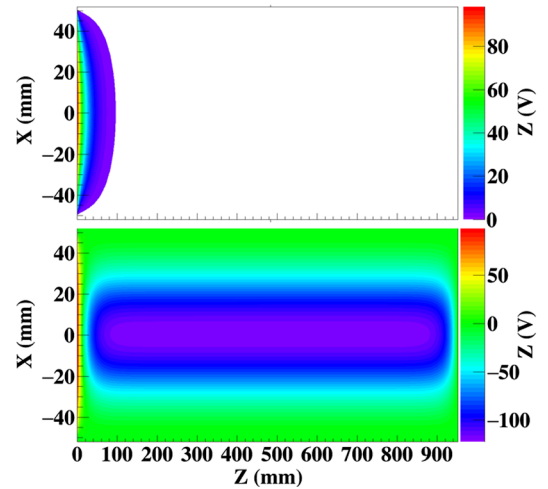


FIG. 1. Laplace solution for beam simulations with boundary conditions (top) and Poisson solution once the beam contribution has been included (bottom).

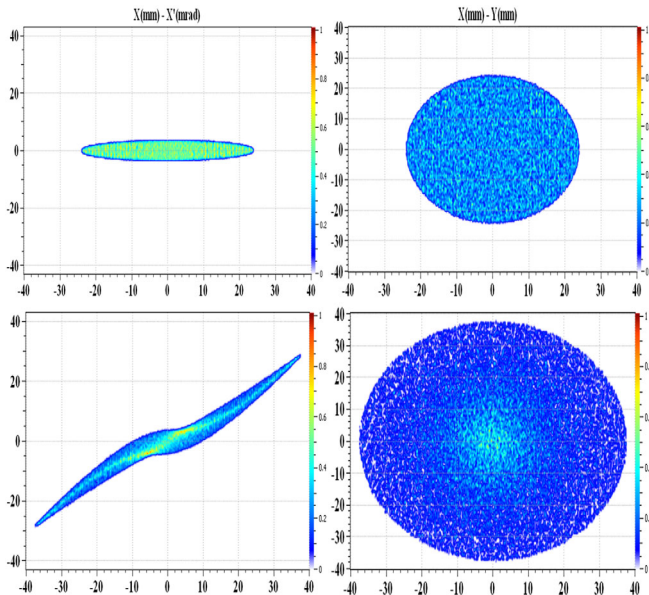


FIG. 2. Input beam distribution (top) and beam at the end of the drift (bottom) after experimenting the SCC for an  $H^-$  beam at 30 mA.

the secondary ions. This model has been used with good matching in IBSIMU and other codes [10,13]. (2) SCC-secondary particle included (SCC-SPI): Once we obtain the Poisson solution for the ion beam, the secondary particles are included in the simulation and the SCC is carried out by its space charge contribution ( $\rho_s$ ), and a new electric potential is created by solving the new Poisson problem  $\nabla^2\phi = -(\rho_s + \rho_b)/\epsilon_0$ . Then the beam is tracked again, and secondary particles are produced again including the secondaries that remain from the previous iteration, this process is made in time steps until reaching the steady state and programmed final time.

The secondary ions are created taking in to account the mean free path of the  $H^-$  beam [4] defined in the previous section. The interactions between the secondary particles and the residual gas has been neglected. The residual gas pressure is taken as constant in all the beam line.

The electric potential boundary conditions set to all the simulations are: at the plane  $z = 0$  (the beam starts at  $z = 0$ ) is set to  $\phi(z = 0) = 100$  V to simulate the beam coming from an Einzel lens and prevent longitudinal secondary ion losses, the end of the line is set to  $\phi = 0$  the typical voltage in the diagnostics devices, and the beam pipe is grounded  $\phi(R) = 0$ .

We use a K-V distribution (Fig 2) as input beam, with 12 mm 1 rms beam size, and Twiss parameters  $\alpha = 0$  and normalized emittance set to 0.2 mm mrad (formed by 80 000 macroparticles). The maximum beam current will be up to 100 mA.

Figure 3 shows the emittance evolution in time recorded at the end of the beam line using the SCC-SPI model where it is possible to appreciate the SCC build-up before the SCC

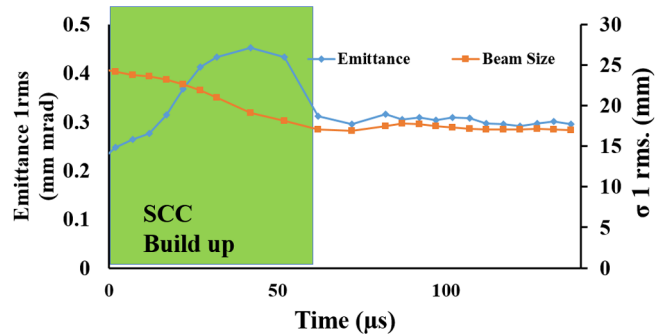


FIG. 3.  $H^-$  emittance and beam size evolution in time due to SCC using the SCC-SPI code for a 30 mA beam with 50 keV energy.

converge to the steady state. This behavior has been compared with experimental measurements in previous works [14].

#### IV. EMITTANCE GROWTH DUE TO SPACE CHARGE

The relation of emittance growth and space charge is difficult to quantify in measurements since the beam emittance increases as we extract more current from the ion source [15]. By considering a beam line section where the input beam parameters are constant and independent of the beam current, we can then quantify the emittance growth in a drift section purely due to space charge repulsion using the net current model.

We performed a beam current scan for  $H^-$ ,  $D^-$ , and  $Li^-$  beams traveling in a 0.5 m drift, where the current varies from 1 mA to 30 mA (limited to have full transmission) for two energies 30 keV and 50 keV (Table I). We used the TRAVEL [16] code and IBSIMU to cross check and both codes have shown similar results.

As it is expected, for all the beams we can observe an emittance growth as the current increases (Fig. 4), but it is limited to less than 1%. Also, between 30 and 50 keV the difference in emittance growth is so small (Fig. 4) that it can be considered as not dependent on the beam energy in that range. These levels of emittance growth will be negligible in any real system. By increasing the current from 1 mA to

TABLE I. Drift simulation input parameters.

Parameter	Value	Units
Emittance	0.20	$\epsilon$ norm. 1 rms (mm mrad)
Energy	30–50	E (keV)
Pressure	5	$\times 10^{-5}$ mbar
Final SCC Level	90	$\eta$ (%)
Drift Length	0.50	L(m)
Drift radius	51	r(mm)

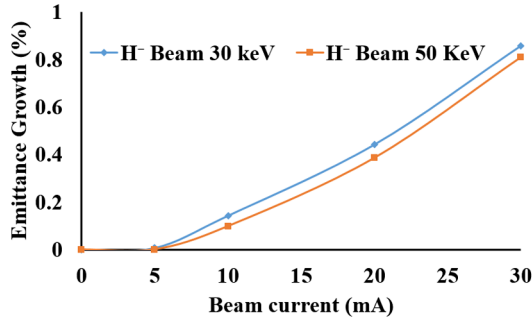


FIG. 4.  $H^-$  emittance growth vs beam current without compensation for a beam with 30 and 50 keV energy in a 0.5 m drift.

30 mA it will generate a more substantial increase in the emittance value that can be attributed to the ion source [15].

### V. EMITTANCE GROWTH DUE TO SPACE CHARGE COMPENSATION

The previous section showed how the emittance suffers small changes as the beam current increases. Now using the SCC-SPI code that includes the secondary ions we will quantify the SCC effect in the same system.

Figure 5 shows that the emittance growth is significantly larger using this method for all the beam ions. In each case, the emittance has been recorded once the SCC process is in the steady state after the SCC build-up.

The emittance growth due to SCC arises from the nonuniform local charge neutralization, induced by the secondary ions radial oscillation around the beam center. In the oscillation the minimum secondary ion velocity is at the edges and the maximum at the beam center, this enhanced the local charge neutralization on the beam edges, producing a nonlinear electric field [3,17].

By increasing the beam current (thereby the potential), the secondary ions also increase its velocity at the beam center, and therefore the difference in speed between the edges and center enhanced the difference in the local charge

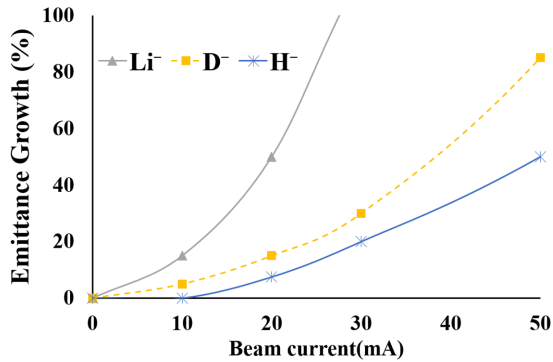


FIG. 5. Emittance growth vs beam current in a 0.5 m drift section using the secondary particles (SCC-SPI) to compensate the 50 keV negative beams.

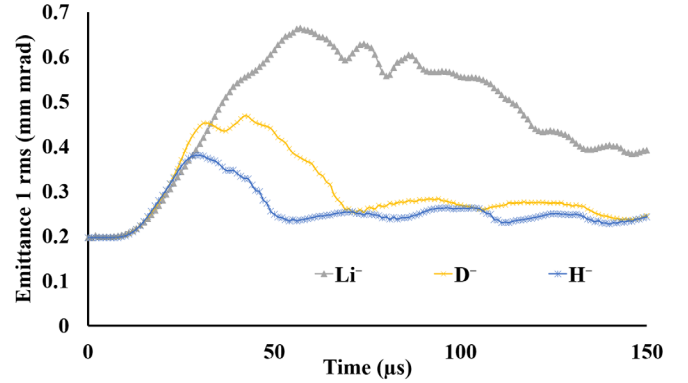


FIG. 6. Emittance time evolution for the 50 keV negative beams in the 0.5 m drift section using the secondary particles to carry the compensation.

neutralization producing a less linear electric field, generating more emittance growth.

Also as the current increases more secondary ions are trapped to compensate the beam. This can be seen as a more uniform compensation. But the fact that there are more ions to neutralize the beam is irrelevant, because at higher currents the dominant effect in the transverse emittance is the secondary ion radial speed.

The fact that the SCC increases the beam emittance above the obtained values for the uncompensated beam in the previous section, it contradicts the idea that the SCC reduce the emittance, but it is true that it helps to transport higher beam intensities by efficiently reducing the Coulomb repulsion.

By increasing the residual gas pressure, it is possible to reduce the emittance growth in the system to levels where it is comparable to the zero SC case [14,18] because as we increase the residual gas pressure the final beam potential decreases to levels where its contribution in the beam dynamics is negligible.

Even when the behavior indicates that the solution to the SCC emittance growth problem is to increase the residual gas pressure, it is not always possible due to pumping constraints or other processes like beam striping that starts to play an essential role in the beam losses or even increase the emittance [18,19].

As Eq. (5) states, from all the studied beams  $Li^-$  shows the longer compensation time due to its bigger mass (Fig. 6). The beam potential depends on the ratio  $\frac{I_b}{v_b}$  and by increasing the mass for fixed energy, the final emittance in steady state increases because its residual potential after the SCC build-up is higher, enhancing the effect of the uneven compensation.

Without the SCC it was not possible to entirely transport more than 20 mA of  $Li^-$  and 30 of  $D^-$  but once the compensation takes place up to 100 mA it can be transported despite the worst emittance.

It is important not to confuse the level of compensation  $\eta$  with the electric potential, for example in the 30 mA  $H^-$

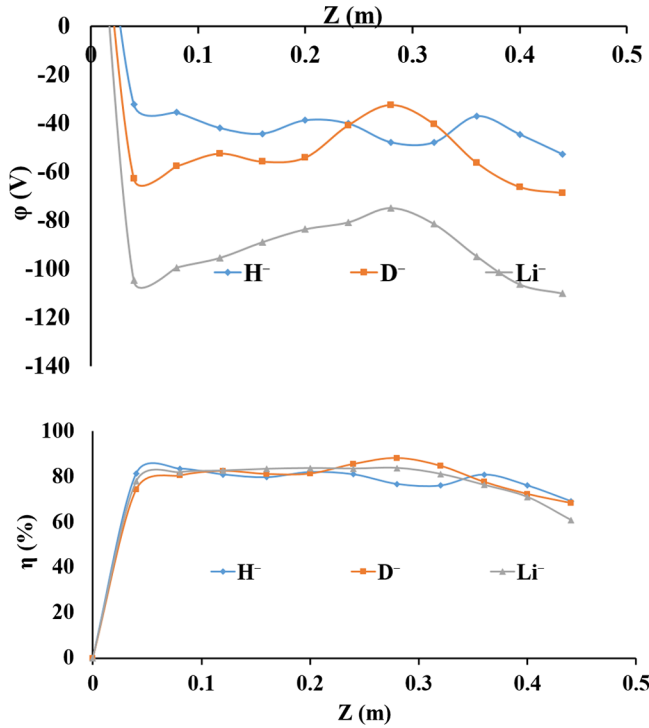


FIG. 7. Beam potential along the line for 30 mA of  $H^-$ ,  $D^-$ , and  $Li^-$  beams (top) and compensation levels for the same ion beams (bottom).

case, the final potential is lower than the  $D^-$  case, hence the bigger potential difference creates a higher emittance growth, but the compensation level for all the ions are the same as can be seen in Fig. 7.

### VI. SCC IN A MAGNETIC CHANNEL

In this section, a solenoid field has been added to a 0.95 m drift to focus the beam and enable the full transport of  $H^-$  and the other negative ions ( $Li^-$  an  $D^-$ ). The solenoid field was modeled in the POISSON superfish [20] code with a total yoke length of 15 cm. Table II shows all the beam line input parameters.

To focus the  $Li^-$  beam the maximum integrated magnetic field ( $\int B^2 dz$ ) along the beam was 48.33  $T^2$  mm, for  $H^-$  and  $D^-$  were 8.32  $T^2$  mm. By tracking the beam through

TABLE II. Simulation input parameters in the beam line including a solenoid magnet.

Parameter	Value	Units
Emittance	0.20	$\epsilon$ norm. 1 rms (mm mrad)
Energy	50	E (keV)
Pressure	5	$\times 10^{-5}$ mbar
Final SCC Level	90	$\eta$ (%)
Drift Length	0.95	L (m)
Drift radius	51	r (mm)

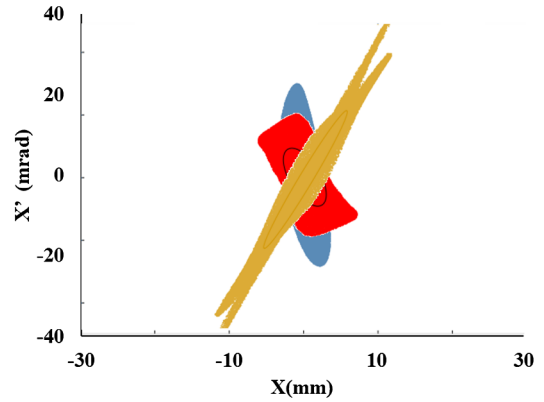


FIG. 8. Transverse emittance at the end of the beam line using the solenoid field for different  $H^-$  beam currents: zero current (blue), 10 mA (red), and 30 mA (yellow).

the solenoid using the net current model, the solenoid induces an emittance growth below 0.5% that can be cataloged as a negligible effect in the emittance for this work. Figure 8 shows the beam transverse emittance when the beam is focused by the solenoid using the SCC-SPI model for different currents.

Only the  $H^-$  has full transmission in the beam line without solenoid field, and the direct comparison between the drift case and using the magnet can be more difficult to illustrate for the other ions. Using the field strength where the final beam size is 12 mm 1 rms with a beam current of 30 mA for all the ions, the  $Li^-$  beam shows the higher emittance growth within the beam line as the drift case.

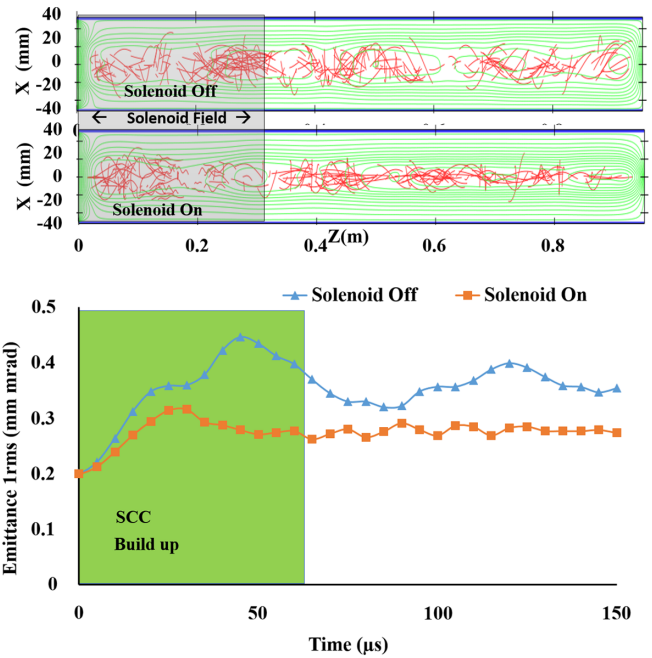


FIG. 9. Secondary ions within the drift (top) and emittance time evolution at the end of the beam line for the 30 mA  $H^-$  beam with the solenoid on and off (bottom).

By increasing the solenoid strength, the emittance starts to decrease and for  $H^-$  it goes from 100% to 50% which is lower than the drift case.

The magnetic field changes the secondary ion dynamics as Fig. 9 shows in the gray region. Without the magnetic field the ions dynamics is dominated by the radial movement around the beam, by adding the solenoid field the secondary ion radial movement is limited and enhance the longitudinal movement.

The change in the secondary ion dynamics impacts in the SCC build-up where the emittance growth is less pronounced before reaching the steady state. As the solenoid strength raises the compensation level and uniformity increases helping to limit the emittance growth (Fig. 9).

### VII. SCC IN THE PRESENCE OF BEAM INSTABILITIES

The SCC-SPI code is capable of simulating situations where the beam itself is not in steady state, making it possible to study three cases of beam instabilities; that often appears during beam operation, and not always it is possible to operate the machine in better beam conditions [2,21]; nevertheless, in all the cases the beam instabilities will be induced once the SCC is in the steady state to avoid the mixture of both effects. In the first instability to be considered the beam intensity will increase. The beam intensity will decay in the second case. Finally, the intensity will drop for a small period to later return to its nominal value.

The Fig. 10 shows the beam pulse profile in time used in simulations, the nominal beam currents vary from 5 to 30 mA and it can rise or decay up to 30%.

#### A. Rising beam intensity

In the first instability to be studied the beam current rises along the pulse [21], as in Fig. 11, by increasing the beam current its electric potential also increases [Eq. (4)], allowing the beam to capture more secondary particles producing a second SCC build-up.

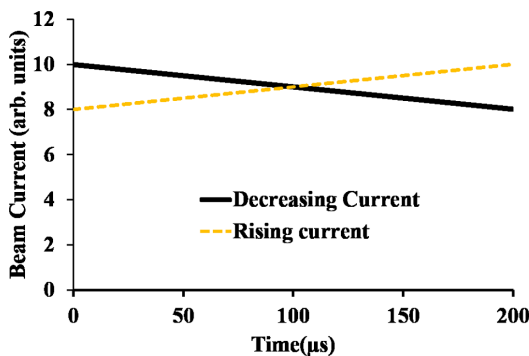


FIG. 10. Beam pulses taken to simulate beam intensity instabilities instead of constant current.

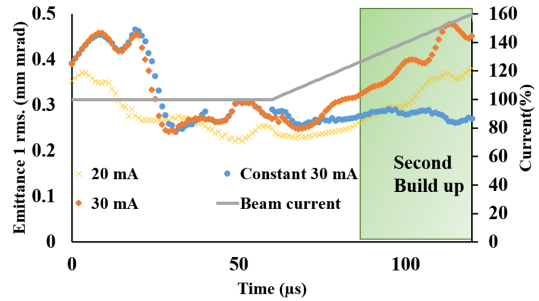


FIG. 11. Beam emittance evolution in time recorded at the end of the line when the beam current is growing.

The slope in the emittance growth depends on how much the beam intensity increases, at 30 mA the build-up is more pronounced than in the 20 mA because there is a greater beam potential to be compensated [Eq. (4)]. The SCC build-up will continue as long as the beam rises because there will always be an extra potential to continue with the secondary ions capture.

Once the current rise stops the length of extension of the second build-up will depend on the residual gas pressure and beam energy.

As expected, once the beam current rise stops, and the build-up finishes the ion capture, in the steady state the beam emittance will converge to the corresponding value for the current defined in the previous section (Fig. 5).

As the nominal beam current decreases, the SCC build-up effect in the emittance will decrease. For cases when the beam current is below 10 mA, the effect is clearly less pronounced than the 30 mA case and its effect is comparable to keep a constant current, this is a consequence that in small currents the space charge is not strong enough to affect the beam particles.

The beam size is one of the most common beam parameters to be measured in an accelerator, and deserves attention. From the recorded beam size at the end of the drift (Fig. 12), the change is more noticeable as we increased the beam current. From 30 to 50 mA, the beam

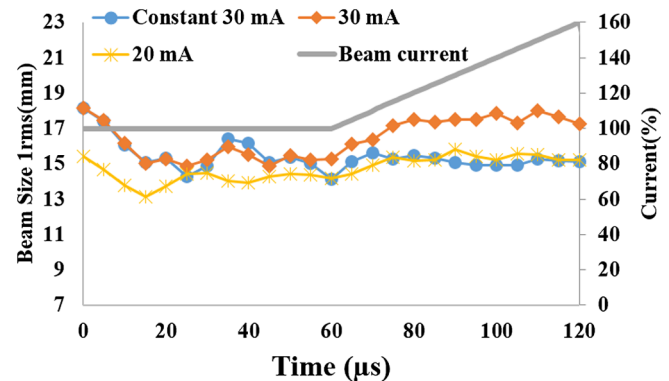


FIG. 12.  $H^-$  beam size evolution when the beam current grows linearly.

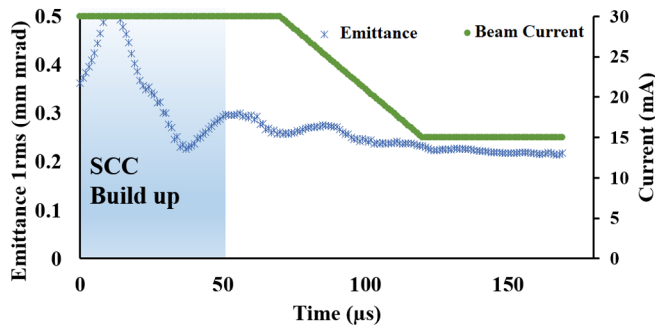


FIG. 13.  $H^-$  transversal emittance evolution under SCC when the beam intensity decays linearly.

size can grow up to 25%, but below 20 mA it is difficult to appreciate differences with the constant current case.

This example shows how the SCC helps to control the maximum beam size, helping to transport higher beam intensities. If it is necessary to avoid beam losses at any cost, this operation case can be a good option even when other beam parameters change.

### B. Decreasing beam intensity

The second case to be simulated is when the beam intensity decays (Fig. 13). If the beam intensity decreases the potential also decreases [Eq. (4)], and less secondary ions are necessary to carry the compensation, the particles that escape from the beam are lost in the vacuum pipe walls. As the beam current decays, the secondary ion losses will continue until the beam stabilizes.

This process is faster than the previous case when the beam current rises because it does not need to create and capture new ions to compensate the beam. Once the current decays stop, the emittance will have the corresponding value to the beam current level defined in the previous section.

The lack of SCC build-up made this case a useful operation mode if the beam pulse is long in comparison to  $\tau$  and is crucial to keep the beam parameters constant, even when it is not possible to maintain a steady beam intensity. Besides these results are independent of the residual gas pressure because of it only losses secondary ions.

### C. Pulsed instability

Now we consider a case where the beam suffers a small drop in the beam current and later the intensity is recovered (Fig. 14). This scenario is a combination of the two cases considered before. At first when the current decreases the beam parameters change quickly to assume the emittance value corresponding the new beam intensity. After being a certain time in a plateau the beam intensity is recovered and it triggers the secondary ions recollection to compensate the beam potential and a second SCC build-up appears. Once again, the severeness and speed of the emittance growth in

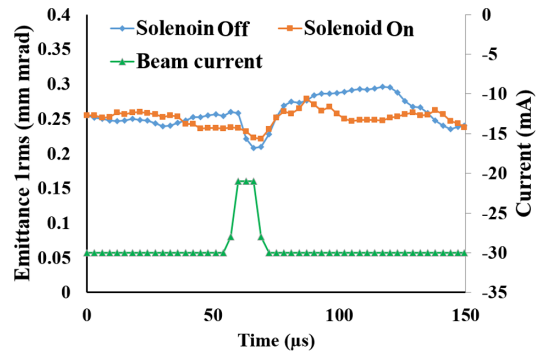


FIG. 14. Emittance evolution under SCC when the beam intensity decay for a short period of time.

the build-up before achieving the normal emittance will depend on the potential that needs to be compensated and the residual gas pressure.

Only if the beam intensity falls more than 30%, it is possible to have a noticeable emittance build-up after the instability occurs as is shown in Fig. 14. Within the pulsed instability the duration of the drop, it will determine how long the beam emittance stays in the corresponding value to the lower beam current.

For beams intensities below 20 mA, the drop induces a change in emittance that it is difficult to appreciate unless it falls more than 40%, which in any case will lead to an unacceptable instability.

As we have seen in previous sections, the inclusion of the solenoid magnet helps to mitigate the emittance growth within the SCC build-up, helping to make its effects less noticeable.

## VIII. CONCLUSIONS

Using 3-D numerical simulations to model the space charge compensation, we studied its effect in the transversal beam emittance in negative ions.

The space charge effect by itself can limit the amount of beam to be transported, but its effect in the emittance is negligible.

If the secondary ions are included in the simulation to carry the SCC, there is a severe emittance growth that can go beyond 100% for beam intensities above 30 mA. Even when the SCC increases the beam emittance, it helps to transport higher beam intensities without losses.

For a fixed energy as the mass of the beam ions increase, the necessary compensation time increases because of the lower ion speed, also the beam potential increases and the SCC generates more emittance growth.

The inclusion of magnetic field changes the secondary ion dynamics helping to reduce the effects of the SCC build-up, and in comparison to the drift case, it reduces the emittance growth in the line.

Once we reach the SCC steady state we studied three form of instabilities for the  $H^-$  beam:

When the beam current increases, it induces a second SCC build-up affecting the beam parameters proportionally to the rise in intensity and residual gas pressure. This operation mode can be used to minimize the beam losses, if the space charge force does not allow to fully transport the beam at the first part of the beam pulse.

The second case studied is when the beam current decreases linearly, the beam parameters quickly change to the one corresponding the new intensity because the system only needs to lose the secondary particles that the potential cannot maintain once the beam current decrease, This case is independent of the residual gas pressure. The effect in the beam size is negligible once the beam is in the SCC steady state.

If the pulse is much longer than  $\tau$ , the second case is more reliable to be used in the ion source operation, because the change in the beam properties is faster and less pronounced, and does not have a build-up that increases the emittance.

In the third case, the beam suffers a temporal drop in intensity, which is a combination of the two modes presented before, this instability can be problematic for beam currents above 30 mA. For lower intensities, it is difficult to notice its effect especially in the presence of magnetic fields.

For the  $H^-$  beam, in the three instabilities cases, their impact on the SCC dynamics is negligible for beams currents below 20 mA, where the current along the pulse changes less than 20%.

### ACKNOWLEDGMENTS

The author would like to thank to Laboratorio Nacional de Supercomputo del sureste de Mexico. This project was supported by Consejo Nacional de Ciencia y Tecnologia (CONACYT).

- 
- [1] C. W. Schmidt and C. D. Curti, A 50-mA negative hydrogen-ion source, *IEEE Trans. Nucl. Sci.* **26**, 4120 (1979).
- [2] R. Keller, R. Thomae, M. Stockli, and R. Welton, Design, operational experiences and beam results obtained with the SNS  $H^-$  ion source and LEBT at Berkeley lab, *AIP Conf. Proc.* **639**, 47 (2002).
- [3] C. A. Valerio-Lizarraga, I. Leon-Monzon, and R. Scrivens, Negative ion beam space charge compensation by residual gas, *Phys. Rev. ST Accel. Beams* **18**, 080101 (2015).
- [4] M. E. Rudd, R. D. DuBois, L. H. Toburen, C. A. Ratcliffe, and T. V. Goffe, Cross sections for ionization of gases by 5-4000-keV protons and for electron capture by 5-150-keV protons, *Phys. Rev. A* **28**, 3244 (1983).
- [5] M. Reiser, *Theory and Design of Charged Particle Beams* (John Wiley and Sons, New York, 1990), p. 248.
- [6] I. A. Soloshenko, Problems of intense negative ion beam transport (invited), *Rev. Sci. Instrum.* **75**, 1694 (2004).
- [7] I. A. Soloshenko, Space charge compensation and collective processes in the intensive beams of  $H^-$  ions, *AIP Conf. Proc.* **380**, 345 (1996).
- [8] T. Tabata and S. Shira, Analytic cross sections for collisions of  $H^+$ ,  $H^{2+}$ ,  $H^{3+}$ ,  $H$ ,  $H^2$ , and  $H^-$  with hydrogen molecules, *At. Data Nucl. Data Tables* **76**, 1 (2000).
- [9] T. Kalvas, O. Tarvainen, T. Ropponen, O. Steczkiewicz, J. Arje, and H. Clark, IBSIMU: A three-dimensional simulation software for charged particle optics, *Rev. Sci. Instrum.* **81**, 02B703 (2010).
- [10] Ø. Midttun, J. Lettry, and R. Scrivens, Measurements of Linac4  $H^-$  ion source beam with a magnetized Einzel lens electron dump, *Rev. Sci. Instrum.* **85**, 02A701 (2014).
- [11] T. Kalvas, O. Tarvainen, T. Ropponen, H. Clark, J. Brinkley, and J. Arje, Application of 3D code IBSimu for designing an H-/D- extraction system for the Texas A&M facility upgrade, in *2nd International Symposium on Negative Ions, Beams and Sources, Takayama, Japan* (2010).
- [12] H. A. van der Vorst, Bi-CGSTAB: A fast and smoothly converging variant of Bi-CG for the solution of non-symmetric linear systems, *SIAM Soc. Ind Appl. Math. J. Sci. Stat. Comput.* **13**, 631 (1992).
- [13] M. Eshraqi, G. Franchetti, and A. M. Lombardi, Emittance control in rf cavities and solenoids, *Phys. Rev. ST Accel. Beams* **12**, 024201 (2009).
- [14] C. A. Valerio-Lizarraga, J. Lallement, I. Leon-Monzon, J. Lettry, O. Midttun, and R. Scrivens, Space charge compensation in the Linac4 low energy beam transport line with negative hydrogen ions, *Rev. Sci. Instrum.* **85**, 02A505 (2014).
- [15] D. A. Fink, J. Lettry, Ø. Midttun, R. Scrivens, D. Steyaert, and C. A. Valerio-Lizarraga, Optimization of the beam extraction systems for the Linac4  $H^-$  ion source, *AIP Conf. Proc.* **1655**, 030006 (2015).
- [16] A. Perrin, J.-F. Amand, and T. Muetze, *Travel User Manual*.
- [17] A. BenIsmail, R. Duperrier, D. Uriot, and N. Pichoff, Space charge compensation studies of hydrogen ion beams in a drift section, *Phys. Rev. ST Accel. Beams* **10**, 070101 (2007).
- [18] A. Misra, A. Goswami, P. SingBabu, S. Srivastava, and V. S. Pandit, Studies on space charge neutralization and emittance measurement of beam from microwave ion source, *Rev. Sci. Instrum.* **86**, 113301 (2015).
- [19] A. L. Zhang *et al.*, Study on space charge compensation in negative hydrogen ion beam, *Rev. Sci. Instrum.* **87**, 02B915 (2016).
- [20] K. Halbach and R. F. Holsinger, SUPERFISH - A Computer Program for Evaluation of RF Cavities with Cylindrical Symmetry, Part. Accel. **7**, 213 (1976).
- [21] H. Ren, S. Peng, Y. XuJie, Z. Chen, T. Zhang, A. Zhang, Z. Guo, and J. Chen, Milliampere  $He^{2+}$  beam generator using a compact GHz ECRIS, *Science China Physics, Mechanics and Astronomy* **56**, 2016 (2013).